Tsunetaka et al. Progress in Earth and Planetary Science (2021) 8:22
https://doi.org/10.1186/s40645-021-00419-6

Progress in Earth and Planetary Science

RESEARCH ARTICLE Open Access

Comparison of length and dynamics of wood pieces in streams covered with coniferous and broadleaf forests mapped using orthophotos acquired by an unmanned aerial vehicle

Haruka Tsunetaka[1*], Slim Mtibaa[1], Shiho Asano[1], Takashi Okamoto[1] and Ushio Kurokawa[2]

Abstract

As wood pieces supplied by landslides and debris flows are one of the main components of ecological and geomorphic systems, the importance of quantifying the dimensions of the wood pieces is evident. However, the low accessibility of disturbed channels after debris flows generally impedes accurate and quick wood-piece investigations. Thus, remote-sensing measurements for wood pieces are necessitated. Focusing on sub-watersheds in coniferous and broadleaf forests in Japan (the CF and BF sites, respectively), we measured the lengths of wood pieces supplied by landslides (> 0.2 m length and > 0.03 m diameter) from orthophotos acquired using a small unmanned aerial vehicle (UAV). The measurement accuracy was analyzed by comparing the lengths derived from the UAV method with direct measurements. The landslides at the CF and BF sites were triggered by extremely heavy rainfalls in 2017 and 2018, respectively. UAV flights were operated during February and September 2019 at the CF site and during November 2018 and December 2019 at the BF site. Direct measurements of wood pieces were carried out on the date of the respective second flight date in each site. When both ends of a wood piece are satisfactorily extracted from an orthophoto acquired by the UAV, the wood-piece lengths at the CF site can be measured with an accuracy of approximately ±0.5 m. At the BF site, most of the extracted lengths were shorter than the directly measured lengths, probably because the complex structures of the root wad and tree crown reduced the visibility. Most wood pieces were discharged from landslide scars at the BF site, but at the CF site, approximately 750 wood pieces remained in the landslide scars approximately 19 months after the landslide occurrence. The number of wood pieces in the landslide scars of the CF site increased with increasing landslide area, suggesting that some wood pieces can be left even if large landslides occur. The lengths and locations of the entrapped wood pieces at both sites were not significantly changed between the two UAV flight dates. However, during this period, the rainfall intensities around the CF site measured by the closest rain-gauge of the Japan Meteorological Agency reached their second highest values from 1976 to 2019, which exceeded the 30-year return period. This suggests that most of the entrapped wood pieces rarely migrated even under intense rainfall.

Keywords: UAV, Wood piece, Debris flow, Landslide

* Correspondence: tsunetakaharuka@ffpri.affrc.go.jp
[1]Forestry and Forest Products Research Institute, 1, Matsunosato, Tsukuba, Ibaraki 305-8687, Japan
Full list of author information is available at the end of the article

1 Introduction

Debris flow causes the entrainment of stand woods located in initiation and riparian zones; consequently, it may include ~10–60% of fluvial wood pieces by volume (Johnson et al. 2000; May and Gresswell 2003a; Lancaster et al. 2003). In addition to destructive impact on life and infrastructure (e.g., Ruiz-Villanueva et al. 2013), wood pieces in a debris flow can alter the flow regime because of their irregular shapes, which can be entrapped around obstacles and lead to anomalous deposition of sediment and inundations (e.g., May 2002; Lancaster et al. 2003; Tang et al. 2018; Booth et al. 2020). The accumulation of wood pieces results in structural peculiarities around channel networks (e.g., Keller and Swanson 1979; Woodsmith and Buffington 1996; Montgomery et al. 1996; Nakamura and Swanson 1993). This contributes to changes in the ecosystem, channel morphology, and sediment flux through logjam formation and the decay of wood pieces (e.g., Wallace and Benke 1984; Lisle 1995; Montgomery et al. 1995; Gurnell et al. 2001; Comiti et al. 2006; Ruiz-Villanueva et al. 2016). Hence, the river form and function are determined by the interaction between water, sediment, and wood (Nakamura et al. 2017; Swanson et al. 2021). Therefore, quantifying wood pieces is important for assessing their impacts on ecological, geomorphological, and fluvial conditions.

Many previous studies focusing on wood pieces in streams have unraveled the role of wood pieces in various spatiotemporal scales and environmental settings (e.g., Nakamura et al. 2017; Swanson et al. 2021), but most of these approaches required direct field measurements such as local monitoring (e.g., Manners et al. 2007), the tracking of wood pieces (e.g., Ravazzolo et al. 2015; Wyżga et al. 2017), and field experiments on artificial wood pieces (e.g., Haga et al. 2002). Taking into account the diversity of forests around channels (e.g., age, species, and density of trees), the monitoring and field survey of wood pieces is evidently an effective approach. However, the necessity of human effort in the field hinders data acquisition in inaccessible areas (e.g., headwater channels and disturbed areas immediately after landslides and debris flows). In practice, field-data acquisition is difficult over large-scale areas exceeding the size of a sub-basin. Therefore, improved field-measurement techniques for wood pieces are urgently required.

To address the measurement issues for wood pieces, remote-sensing approaches using three-dimensional data have been applied. The use of LiDAR (light detection and ranging) data clearly reduces the processing time required for mapping logjams and individual wood pieces (Kasprak et al. 2012; Abalharth et al. 2015; Atha and Dietrich 2016). However, this technology is expensive and is therefore available only in some regions. Alternatively, photogrammetry based on structure from motion multiview stereo (SfM-MVS) using images captured by an unmanned aerial vehicle (UAV) can produce three-dimensional data (e.g., digital surface models and point clouds), which has been proven to be more time-efficient than classical field surveys (Sanhueza et al. 2019). This approach overcomes data availability issues and is relatively low cost. Nevertheless, most tests have been conducted in lowlands and flood plains rather than in low-accessibility areas such as steep channels (e.g., Sanhueza et al. 2019). As the accuracy of three-dimensional data acquired by SfM-MVS is greatly influenced by complex surfaces and obstacles—steep slopes, large reliefs, and vegetation coverage (e.g., Fonstad et al. 2013; James and Robson 2014)—many unresolved uncertainties remain in SfM-MVS analyses of three-dimensional data of wood pieces in steep and complex areas such as channels impacted by landslides and debris flows.

Aerial photography is a traditional source of two-dimensional data that may provide more-or-less meaningful information about wood pieces. Even satellite images from Google Earth are being used for accurate wood-piece mapping (Atha 2013; Ulloa et al. 2015). Hence, the efficacy of aerial photography is evident, but the accuracy and effort of mapping depend on the image quality. In this respect, it is expected that small UAVs may allow the acquisition of high-resolution aerial photographs at low cost because of the lower flight altitudes and higher portability of UAVs than conventional manned aerial vehicles. Moreover, because flights of small UAVs can overcome inaccessibility issues and cover several kilometers on the horizontal scale (depending on the flight design), a UAV is a fairly attractive tool for obtaining wood-piece measurements in low-accessibility areas.

In addition, wood pieces are often quickly removed by river administrators to avoid unexpected damages in the downstream area resulting from its transport by streamflow after being supplied and entrapped in streams (hereinafter this is referred to as secondary transport). The risk arising from the secondary transport of wood pieces (e.g., damages on facilities in residential regions) has not been evaluated properly so far because it has been difficult to conduct field surveys of the wood-piece supply immediately after intense rainfall. In contrast, UAV flights can be conducted immediately after rainfall events that result in a large number of wood pieces in channels, which can potentially contribute to unraveling wood-piece dynamics after their supply and entrapment. Therefore, an efficient mapping method of wood pieces enables the investigations of wood-piece transport due to subsequent rainfall, even if it is carried out with a simple method using aerial photography. Nevertheless,

the potential to measure wood pieces based on aerial photographs acquired using UAV has not been thoroughly examined due to lack of sample cases.

In this study, we analyze the accuracy of UAV-based measurements for wood-piece lengths. Two regions in Japan are selected representing two forest types, coniferous and broadleaf forests. In both regions, a large number of wood pieces were supplied to streams through landslides and debris flows triggered by a single rainfall event. This research has two main objectives: (1) to analyze the capability of orthophotos acquired via UAVs and hence measure the lengths of wood pieces and (2) to investigate whether entrapped wood pieces move again in subsequent rainfall. Based on the results, we discuss the effectiveness of UAV measurements and how wood pieces behave after their entrapment.

2 Study sites

To examine the influence of tree type on the accuracy of wood-piece measurements obtained using the orthophotos acquired by the UAV, we selected two different sites covered by different forest types (coniferous and broadleaf) in Japan (Fig. 1a). Hereafter, the former site is referred to as the CF (coniferous forest) site (Fig. 1b), whereas, the latter site is referred to as the BF (broadleaf forest) site (Fig. 1c). In this study, we use the term "tree type" to indicate either coniferous or broadleaf trees rather than the detailed tree species.

2.1 Coniferous forest site

The CF site is a sub-watershed of the Otoishi watershed located in the northern part of Kyushu Island, Japan (Fig. 1a, b). Its highest point is approximately 385 m above sea level (a.s.l.), and its lowest point is approximately 225 m a.s.l. The total length of the main channel is approximately 760 m with an average slope of approximately 12° (before the debris-flow occurrence), and the drainage area is approximately 0.15 km^2. To prevent the destabilization of hillslopes and banks, five closed-type check dams (check dams without slit and steel lattice structures for trapping wood pieces and boulders, e.g., Piton and Recking 2016) were constructed before the debris flow occurred in 2017 (Fig. 2a). Most hillslopes are covered with artificial coniferous forests that consist mainly of *Cryptomeria japonica* and *Chamaecyparis obtusa*. The tree heights range from approximately 15 to 25 m.

In the region around the CF site, an intense rainfall on July 5, 2017, triggered more than 2000 landslides, which transformed into debris flows, resulting in a large number of wood pieces (Chigira et al. 2018). The rainfall event that triggered these landslides has been recognized as extremely heavy rainfall that led to intense rainfall intensity over 9 h in nearly the same location (Kato et al. 2018). This event resulted from extremely tall convection (Tsuji et al. 2020) generated by organized mesoscale convective systems (Unuma and Takemi 2021) and increased atmospheric moisture convergence due to global warming (Imada et al. 2020). The sliding sediment layers were mainly granodiorite and pelitic schist (Chigira et al. 2018). The intense rainfall in July 2017 triggered six landslides at the CF site (Fig. 2a), but the existing check dams effectively prevented the descent of sediment and wood pieces. Hence, most of the wood pieces were trapped around the check dams and along the channel, thereby preventing damage in the downstream residential areas. Because of this low impact on the residences, the wood pieces were not removed and were left in situ until the time we carried out observations.

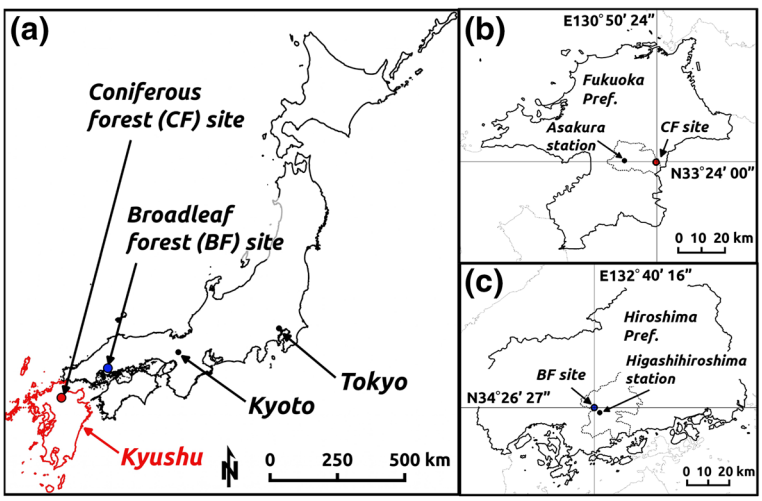

Fig. 1 Study site: **a** overview, **b** locations of the coniferous forest (CF) site and the rain-gauge station (Asakura station), and **c** locations of the broadleaf forest (BF) site and the rain-gauge station (Higashihiroshima station)

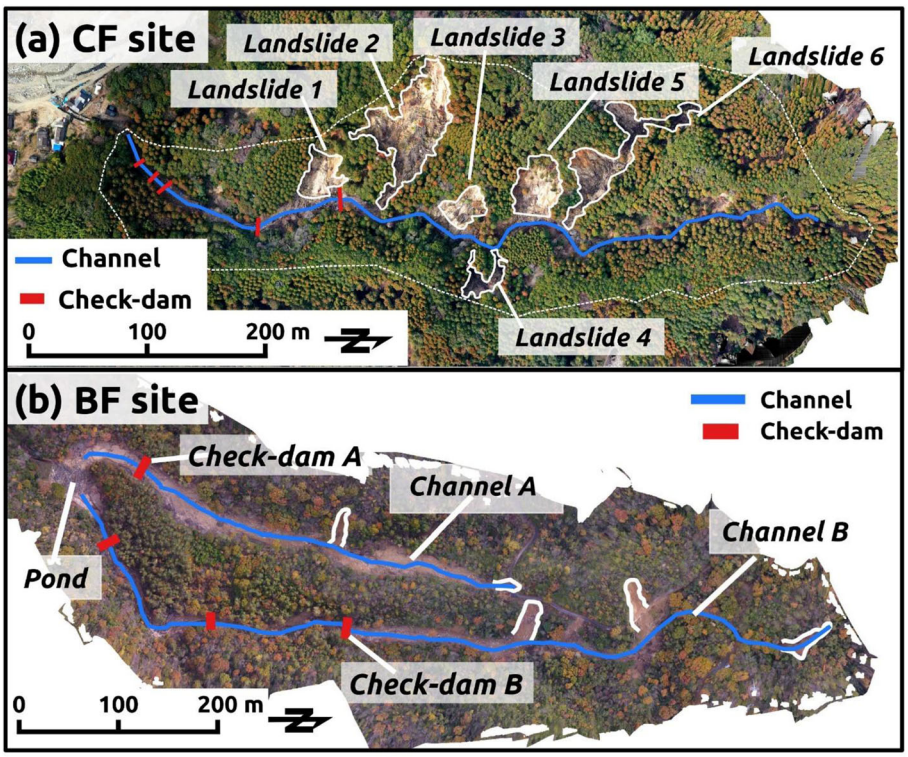

Fig. 2 Orthophoto of the study sites: **a** the coniferous forest (CF) site and **b** the broadleaf forest (BF) site. The right side indicates the upper part of the channel (i.e., the streams descend from north to south). The white solid lines indicate the landslide scars. The white dotted line in panel **a** indicates the boundary of sub-watershed

2.2 Broadleaf forest site

The BF site is located in Hiroshima Prefecture in the western part of Japan (Fig. 1c). Here, two channels are confluent at an irrigation pond that is located at the lower ends of channels (~305 m a.s.l., Fig. 2b). The highest points of channels A and B are ~410 and ~480 m a.s.l., respectively. Their total lengths are ~880 and ~466 m, respectively. The average slopes of the two channels are similar, at ~11–12° (before the debris flow occurrence). The drainage areas of channels A and B are ~0.07 and ~0.13 km^2, respectively. Similar to the case of the CF site, four closed-type check dams were constructed before the debris flow occurred in 2018 (Fig. 2b). The forest type completely differs from that at the CF site, and most of the hillslopes are covered by broadleaf forests with various tree types. The tree heights range from approximately 10 to 20 m.

In the west part of Japan, a stationary front affected by Typhoon Prapiroon caused heavy rainfall on July 5–7, 2018 (Tsuguti et al. 2019), and triggered approximately 8000 landslides in Hiroshima Prefecture due to the vulnerable geological setting, which is dominated by weathered granite (Kaibori et al. 2018). The extremely heavy rainfall event that triggered these landslides resulted in high rainfall intensity over 72 h (Sueki and Kajikawa 2019), probably due to anomalies in temperature and specific humidity (Tsuji et al. 2020) arising from mesoscale convective systems (Unuma and Takemi 2021) and global warming (Imada et al. 2020). Five landslides occurred at the BF site (Fig. 2b), but the check dams and the pond effectively prevented the descent of sediment and wood pieces. Similar to the situation at the CF site after the disaster, the wood pieces produced in the BF site were left in situ until we carried out the observations.

3 Methods

This study consists of two parts: (1) an assessment of the accuracy of the wood-piece measurements obtained from ortho-photography acquired via the UAV and (2) a rainfall analysis to investigate the possible transport of entrapped wood pieces.

3.1 UAV flights and aerial-photograph processing

A small consumer-grade UAV (DJI Mavic 2 pro; Table 1) was used for the flights covering the channels and landslides (Fig. 2). Two UAV flights were conducted at each of the respective study sites (Table 2): (1) February 14 and September 26, 2019, at the CF site and (2) November 16, 2018, and December 25, 2019, at the BF site. The flights

Table 1 Properties of the UAV and the installed camera

UAV	
Model	DJI Mavic 2 pro
Weight	907 g
Diagonal size	354 mm
Max. duration of flight	31 min
Camera	
Number of pixels	20 M
Sensor size	13.2 × 8.8 mm
Focal length	∞

were conducted manually at heights above ground between approximately 50 and 150 m, and most of the photographs were taken in the nadir direction. The flight path provided at least 70% overlaps in the forward and side directions of the aerial photographs. To reduce the differences in shade and brightness among the acquired aerial photographs, the flights were operated avoiding strong sunlight.

The acquired images were processed using the SfM-MVS photogrammetry software (Agisoft, Metashape Professional version 1.5.1). Usually, artificial reference markers are established, and their absolute coordinates are measured with a GNSS (global navigation satellite system), providing ground control points (GCPs) for geo-referencing the SfM-MVS photogrammetry (e.g., Barnhart et al. 2019; Tsunetaka et al. 2020). However, immediately after a debris-flow disaster, the establishment of artificial reference markers is impeded by wood pieces, which behave as obstacles. The recently developed, high-accuracy, RTK (real time kinematic) GNSS-based direct geo-referencing system built into a UAV for SfM-MVS photogrammetry processing makes it possible to obtain accurate absolute coordinates without GCPs (e.g., Carbonneau and Dietrich 2017). However, it is an expensive technology, and the consumer-grade UAV that we used does not include such an RTK-GNSS system. Because of these operational limitations, we focused on the ability to make wood-piece measurements using relatively low-cost UAV-based processing. Our intention was thus to assess the accuracy of measurements using only UAV flights without any other field operations (e.g., setting artificial reference markers) or RTK-GNSS systems.

Table 2 Dates of UAV flights and number of aerial images used to provide orthophotos

	Date	Number of aerial images
CF site		
First flight	February 14, 2019	159
Second flight	September 26, 2019	284
BF site		
First flight	November 16, 2018	315
Second flight	December 25, 2019	141

The position data from the built-in GNSS that controlled the flight position were contained in exchangeable image file format data for each photograph. Using these data, we preliminarily collected the coordinates of the processed orthophotos. Following standard SfM-MVS photogrammetry workflow, the orthophotos were produced with a spatial resolution of 0.03–0.05 m. Because the measurements were performed without establishing artificial reference markers, the coordinates of the resulting orthophotos taken during the different flight dates did not overlap accurately. As the principal aim of using sequential orthophotos was to investigate the transport of the wood pieces, it is necessary only to have relative coordinate system overlap (i.e., absolute coordinate system overlap is not required). Thus, we manually adjusted two sequential orthophotos using the crests of the check dams as GCPs for which the coordinates were taken from the older orthophoto. Using the extracted coordinates, the orthophoto acquired on the later date was transformed to fit the first one. The differences in the lengths of selected immobilized objects (e.g., large boulders and the crests of check dams) were less than approximately 0.2 m. Therefore, we considered the horizontal accuracy of the orthophotos to be less than 0.2 m.

3.2 Accuracy assessment

Because we used orthophotos (i.e., two-dimensional data) to quantify the wood pieces, the dimension of wood pieces measured by the UAV is its length. First, we extracted the length of the wood pieces, both as a single piece and as an element of a jam-forming log as line data from the acquired orthophotos. Note that invisible wood pieces below a jam-forming log are out of the measurement target. All visible wood pieces were extracted at the CF site (the area surrounded by the dotted white line in Fig. 2a), whereas only wood pieces around check dams A and B were investigated at the BF site because of the low visibility of wood pieces originating from broadleaf trees (Fig. 2b). Accordingly, the measurement range differed from a reach scale at the BF site to a sub-watershed scale at the CF site.

The measurement accuracy of the extracted length is presumably affected by visibility, which is related to the types and sizes of the trees (e.g., length and diameter). Moreover, because wood pieces are often inclined and broadleaf trees have a curved shape, orthogonal projection to obtain the extracted length may cause a measurement error (Fig. 3). Hence, we focused on the differences among the tree types (i.e., coniferous or

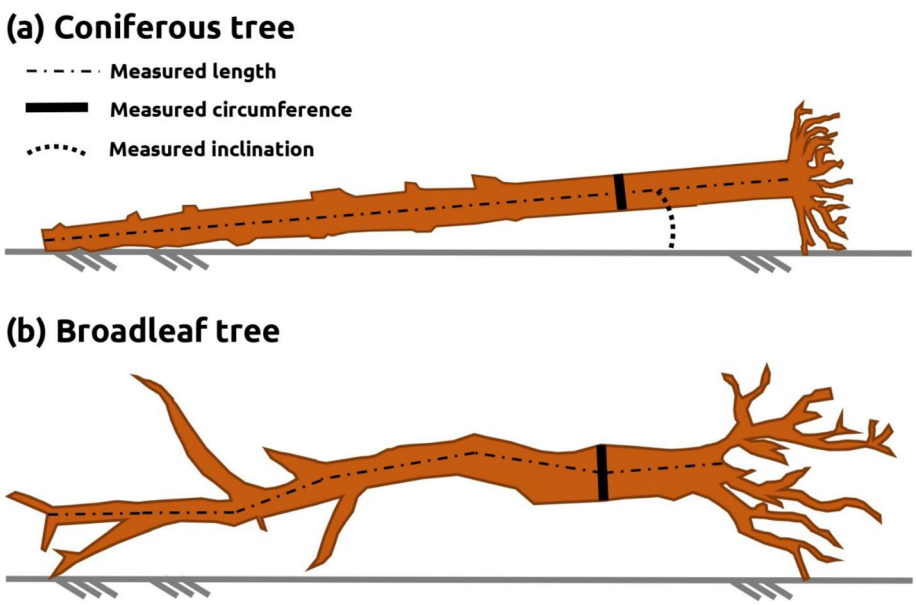

Fig. 3 Schematic representation of the components for the direct measurement of wood pieces: **a** the coniferous tree and **b** broadleaf tree. The left side indicates the top of each type of tree (the side of the tree crown). The right side depicts the root wad

broadleaf trees), diameters, and entrapment inclinations of the wood pieces.

To compare with the extracted lengths of the wood pieces, we directly measured wood pieces at the study sites (Fig. 3). Based on the orthophotos from the first flight, the visible wood pieces were labeled. When we conducted the second flight, we found and directly measured some of the labeled wood pieces (50 wood pieces at the CF site on September 26, 2019, and 131 wood pieces at the BF site on December 25, 2019). In the found wood pieces, we measured the lengths—excluding the root wads and twigs—directly using a tape (estimated precision < 0.05 m) (Fig. 3), similar to the approach of Sanhueza et al. (2019) and compared those measurements with the lengths extracted from the orthophotos from the first UAV flight. Using the same tape, we measured the circumferences of the found wood pieces at approximately 1.0–1.5 m height from the root wad. For wood pieces less than approximately 1.5 m in length, because there were only slight differences in the thickness of a single fragment, we measured the circumference at an arbitrary location. From the measured circumferences, we calculated the diameters of the found wood pieces. Note that, because the minimum measurable circumference was approximately 0.1 m, some of the calculated diameters of the wood pieces were smaller than the estimated precision of the tape measurement (0.05 m). At the CF site, as the wood pieces retained relatively straight shapes, the entrapment inclination was measured directly using an angle meter (estimated precision < ±1°, Fig. 3a).

The extraction of wood pieces depends on its visibility in the orthophotos, and thus, the identification of its origin as well as the detection of small wood pieces of less than the minimum resolution of the orthophotos (i.e., 0.03 m in diameter) was beyond the measurement purpose. In addition, the successful extraction of wood pieces from the orthophotos was constrained by the visibility of the wood-piece length, not by the visibility of the wood-piece width (diameter). Considering the horizontal accuracy of the orthophotos (< 0.2 m), the minimum length of the extracted wood pieces was set to 0.2 m. A "large wood" piece is typically defined as a wood piece > 0.1 m in diameter and > 1 m in length (e.g., Jackson and Sturm 2002; Tang et al. 2018). Note that, our dataset included small wood pieces (> 0.03 m in diameter and > 0.2 m in length) because of the minimum measured diameters and the lengths of the wood pieces. Moreover, the extracted wood pieces may contain multiple pieces that originated from a single tree. Note that, as a single stand wood may result in several wood pieces, counting the extracted wood pieces involves uncertainty.

3.3 Analysis to determine the transport of wood pieces

To analyze whether or not wood pieces migrated through time, we created the quantile–quantile (Q–Q) plots of the probability density of the extracted length. The CF site was divided into seven zones: six landslide scars and the riparian zone with a channel approximately 760 m in length (Fig. 2a). Changes in the probability density of the wood-piece length were visually tested using the Q–Q plots. Similarly, Q–Q plots were

made for channels A and B at the BF site (Fig. 2b). For each zone, to investigate the coincidence of the probability density of the extracted length between the two flight dates (Table 2)—(1) February and September, 2019 (i.e., approximately 7 months), at the CF site and (2) November, 2018, and December, 2019 (i.e., approximately 13 months), at the BF site—we conducted a goodness-of-fit test using the Kolmogorov–Smirnov test (e.g., Sane et al. 2018).

In addition, we investigated whether specific rainfall characteristics triggered the secondary transport of wood pieces. For this reason, we used the hourly rainfall records from 1976 to 2019 obtained at the closest rain gauges installed by the Japan Meteorological Agency, the Asakura station (for the CF site, Fig. 1b) and the Higashihiroshima station (for the BF site, Fig. 1c). The annual maxima of rainfall intensity of various durations (1, 2, 3, 6, 12, 24, 48, and 72 h) were investigated from 1976 to 2019 and compared with the intensity of the rainfall that triggered the debris flows. In addition, we examined the records of rainfall maxima after the debris-flow occurrence. The return periods were calculated based on the probability density of each rainfall intensity fitted by a Gumbel distribution based on the annual maxima (e.g., Koutsoyiannis et al. 1998; Sane et al. 2018). For this fitting process, the goodness-of-fit test (Kolmogorov–Smirnov test) resulted in *p*-values exceeding 0.1, suggesting that the applied Gumbel distribution models well fitted the probability density of the observed rainfall.

4 Results

4.1 Lengths of the entrapped wood pieces

As expected, a comparison of the extracted and measured wood-piece lengths indicates that the measurement accuracy depends on the visibility of the wood pieces. Fifty wood pieces were directly measured at the CF site (Fig. 4a). Fourteen of them were trapped by stand woods located in the riparian zone, and they were partially invisible from the sky due to the coverage by the tree crowns. This low visibility caused underestimates of the extracted lengths, with errors in length being a maximum at ~10 m. In contrast, 36 other pieces were fully visible, and their lengths ranged between about 3 and 22 m. Despite this wide range, most measurements coincided well with the extracted lengths. This clear dependence on the visibility of the wood pieces is reflected in the boxplot (Fig. 5), indicating that the interquartile ranges obviously differed between the visible and covered wood pieces; the differences ranged from −0.4 to 0.5 m and from 1.6 to 4.3 m, respectively (Fig. 5).

The lengths of 130 wood pieces without crown coverage were directly measured at the BF site, but they rarely coincided with the extracted lengths, which were usually underestimates (Fig. 4b). Moreover, the differences between the lengths varied. The related interquartile range varied between approximately 0.3 and 2.1 m, reflecting the lower accuracy and higher uncertainty when measuring broadleaf trees than when measuring coniferous trees (Fig. 5).

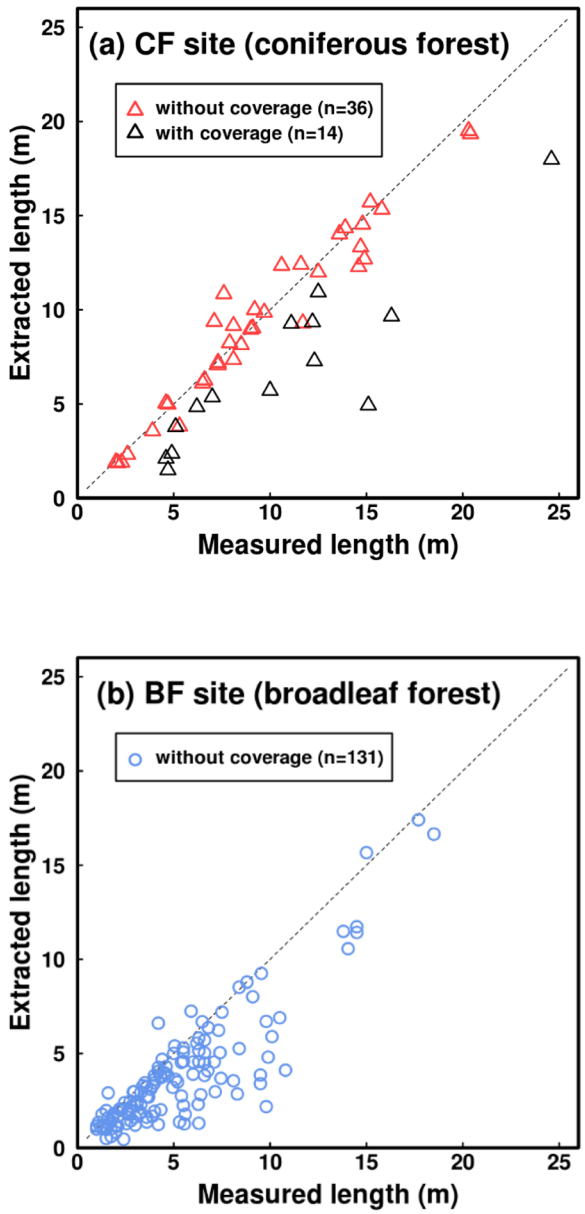

Fig. 4 Comparison between extracted and measured lengths of wood pieces: **a** the coniferous forest (CF) site and **b** the broadleaf forest (BF) site

Strictly speaking, the extracted length was the orthogonally projected length, and we therefore calculated the slope distance of the measured wood pieces from the extracted length using the measured slope. However, this correction did not significantly improve the measurement accuracy because differences in the

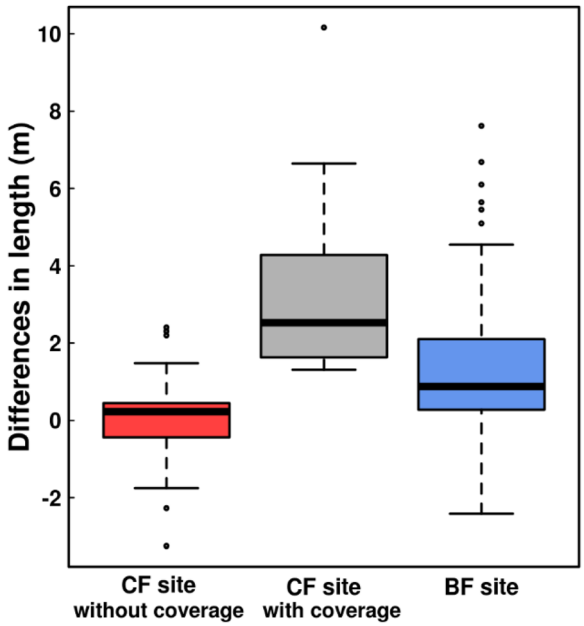

Fig. 5 Boxplot of differences between the extracted and measured lengths of the wood pieces. Differences in length were calculated by subtracting the extracted length from the measured length

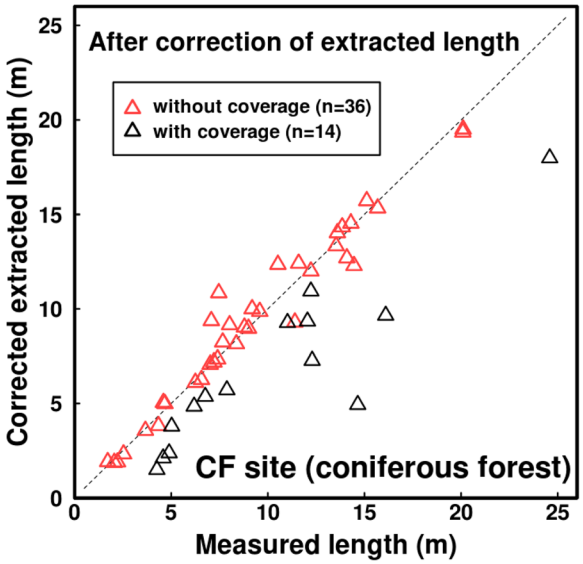

Fig. 6 Comparison between corrected extracted length and measured length of the wood pieces at the coniferous forest (CF) site. The corrected extracted length indicates that the inclined length was corrected from the extracted length (i.e., orthogonally projected length) using the directly measured inclination of the wood pieces

visibility of the wood pieces depending on the difference in the tree types overwhelmed the influence arising from the approximation by the orthogonal projection (Figs. 4a and 6). The differences in the wood-piece diameters indicate that the extracted lengths of relatively narrow pieces (< ~0.2–0.3 m in diameter) at the BF site tend to be underestimated (Fig. 7), despite the absence of crown and logjam coverages. Note that, especially for wood pieces with diameters less than 0.1 m, direct measurements (estimated precision < 0.05 m) and orthophotos (estimated precision < 0.2 m) can contain significant measurement error independent of the differences in tree types. However, even for wood pieces with diameters between 0.1 and 0.2 m, the measurement errors were higher at the BF site than at the CF site (without coverage, see Fig. 7). This suggests that the decreased visibility of small-diameter pieces was responsible for the decreased measurement accuracy at the BF site.

Most wood pieces were discharged from landslide scars at the BF site, whereas a total of approximately 750 wood pieces (exceeding 50% of the total of ~1370 wood pieces) were left in the landslide scars at the CF site. At the CF site, the interquartile of the wood-piece length differed slightly among the landslide scars, but they were similar between the riparian zone and the average of all landslides, 2.5 to 7.7 m and 2.6 to 8.3 m, respectively (Fig. 8a). The median length of the wood pieces ranged from 3.4 (in landslide 4) to 7.8 m (in landslide 1). At the BF site, the interquartile of the wood-piece length at check dams A and B were 1.1 to 3.1 m and 0.8 to 2.6 m, respectively (Fig. 8b). The median lengths of the wood pieces at check dams A and B were similar: 1.8 and 1.5 m, respectively. The median wood-piece length at the

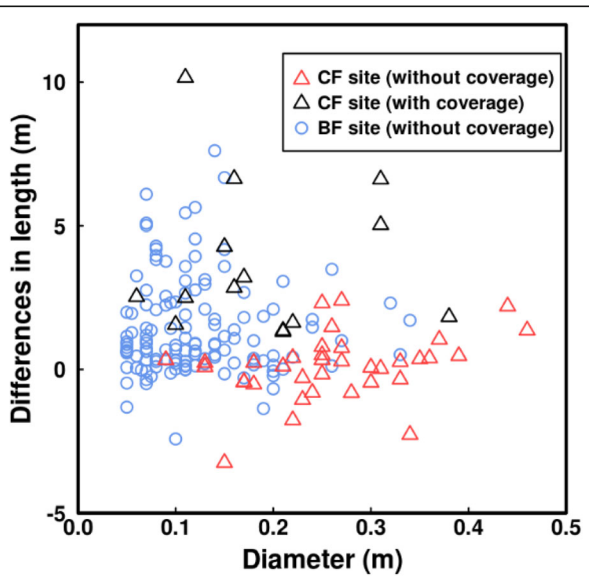

Fig. 7 The differences between the extracted and measured lengths of the wood pieces at both broadleaf forest (BF) and coniferous forest (CF) sites as functions of the measured diameter. Differences in length were calculated by subtracting the extracted length from the measured length, similar to Fig. 5

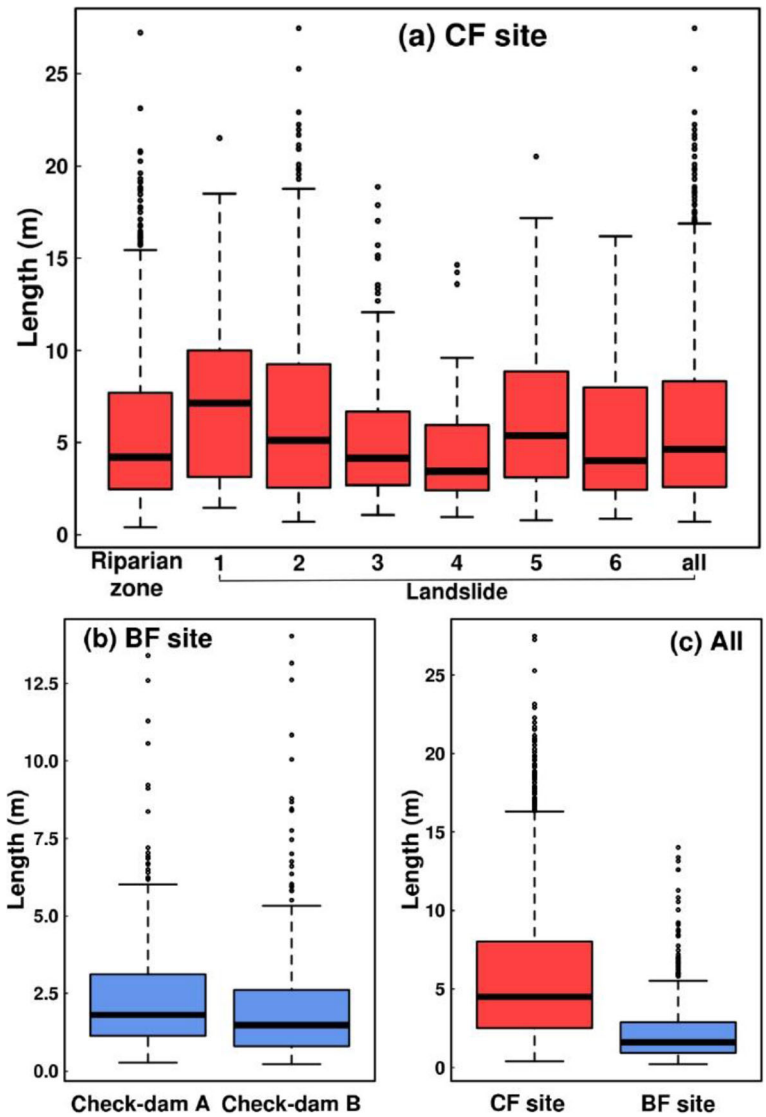

Fig. 8 Boxplots of the extracted lengths: **a** the coniferous forest (CF) site, **b** the broadleaf forest (BF) site, and **c** all measured lengths. In panel **a**, the labels of the landslides correspond to Fig. 2a ("All" indicates the total number of landslides). The wood piece extracted in the area excluding landslide scars was regarded as the riparian zone (Fig. 10)

CF site was ~4.5 m, which is evidently greater than that at the BF site (Fig. 8c).

The areas of the landslide scars at the CF site ranged widely, from ~800 to 5400 m^2 (Fig. 9). The number of entrapped wood pieces tended to increase with the increase in the area of the landslide scars (Fig. 9). Landslide 2 (~5400 m^2) accounted for approximately 40% of the total area of the landslide scars (i.e., the total landslide area at the CF site is ~14,000 m^2), and thus, this landslide was the predominant sediment source at the CF site. Despite this huge sediment discharge, the number of entrapped wood pieces was highest among the landslide scars, at approximately 350 wood pieces.

4.2 Transport of entrapped wood pieces

At both sites, there were only slight visible changes in the spatial distribution of the wood pieces between the two orthophotos (Figs. 10 and 11). The wood pieces were trapped in various areas—for instance, as wood pieces in the riparian zone, the check dams, and the landslide areas. Despite these differences in the entrapment zones, it seems that most of the wood pieces did not move even after about 7 months (at the CF site, Fig. 10) and over 1 year (at the BF site, Fig. 11). The Q–Q plots indicate that the probability density of the extracted wood-piece length coincided well with the measured length, regardless of the division of the entrapment zones (Fig. 12). Thus, the *p*-

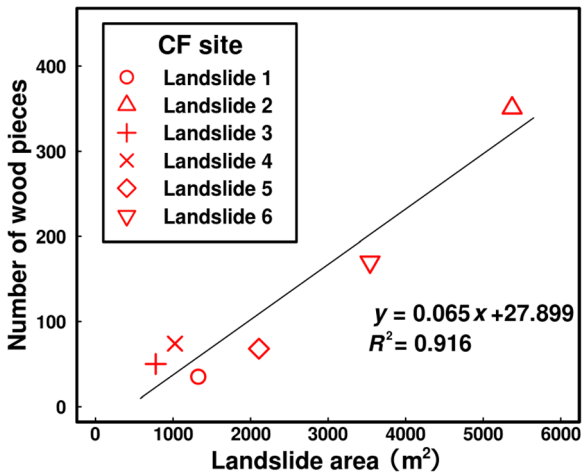

Fig. 9 Comparison between landslide area and the number of remaining wood pieces at the coniferous forest (CF) site. The black line is the linear regression line

values in the goodness-of-fit test exceeded 0.05, suggesting that the changes were statistically insignificant.

The rainfall anomalies that triggered debris flows were revealed by comparing the annual maxima of the rainfall intensity in each case. At the CF site, the rainfall that triggered the debris flow in 2017 was obviously excessive rainfall, as the rainfall intensity was the highest compared with the annual maxima of other years, regardless of the rainfall duration (Fig. 13a). This suggests that the highly intense and continuous rainfall resulted in the large number of wood pieces. At the BF site, for the rainfall that triggered debris flows in 2018, rainfall intensities with 1–6 h durations were not higher than the other annual maxima since 1976, but those with 12–72 h durations were the most intense since 1976 (Fig. 13b). This suggests that a high rainfall intensity continuing over 12 h resulted in landslides and debris flow accompanied by the propagation of wood pieces. Both rainfall events that triggered debris flows at the CF and BF sites reached levels exceeding the 100-year return period (Tables 3 and 4).

At the BF site, after the landslides and debris flows in 2018, the maximum annual rainfall intensity in 2019 was not remarkable (Fig. 13b, Table 4). Thus, although most wood pieces remained in place, it is difficult to analyze the potential of secondary transport of entrapped wood pieces via intense rainfall. In contrast, at the CF site, after the landslides and debris flows in 2017, the annual rainfall intensity maxima in 2018 and 2019 were the second or third highest values since 1976 (Fig. 13a). Although the intensity of the triggering rainfall in 2017 significantly exceeded the annual maxima in 2018 and 2019 in terms of the return period, some rainfall intensities in 2018 and 2019 exceeded the level of the 30-year return period (Table 3). Such a heavy rainfall event occurred on July 21, 2019 (between the UAV flights at the CF site; Table 2).

5 Discussion

5.1 Implications for UAV-based wood-piece mapping

Our results demonstrate that the visibility and tree types of the wood pieces determine the ability to measure

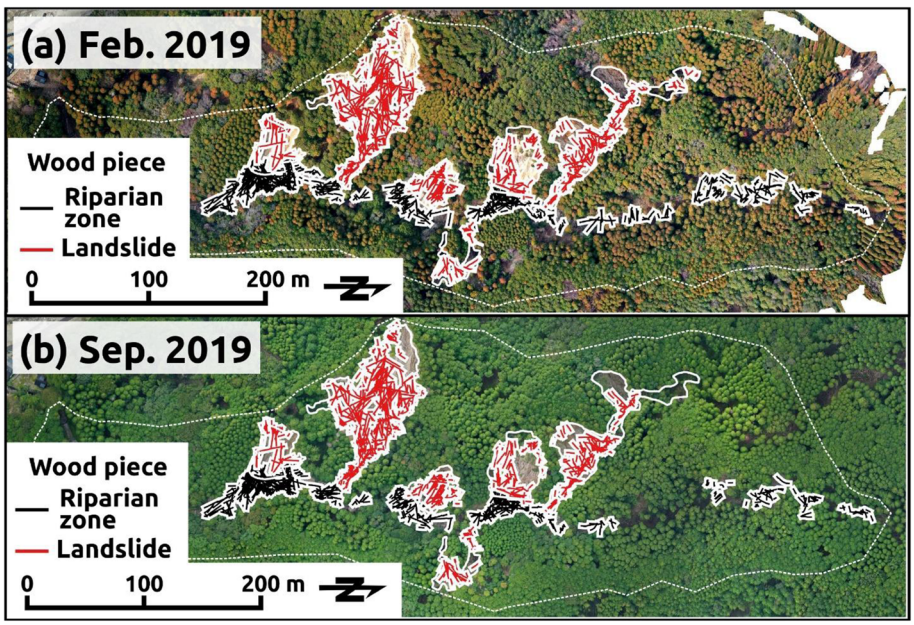

Fig. 10 Spatial distribution of extracted wood pieces at the coniferous forest (CF) site: **a** February 14, 2019, and **b** September 26, 2019

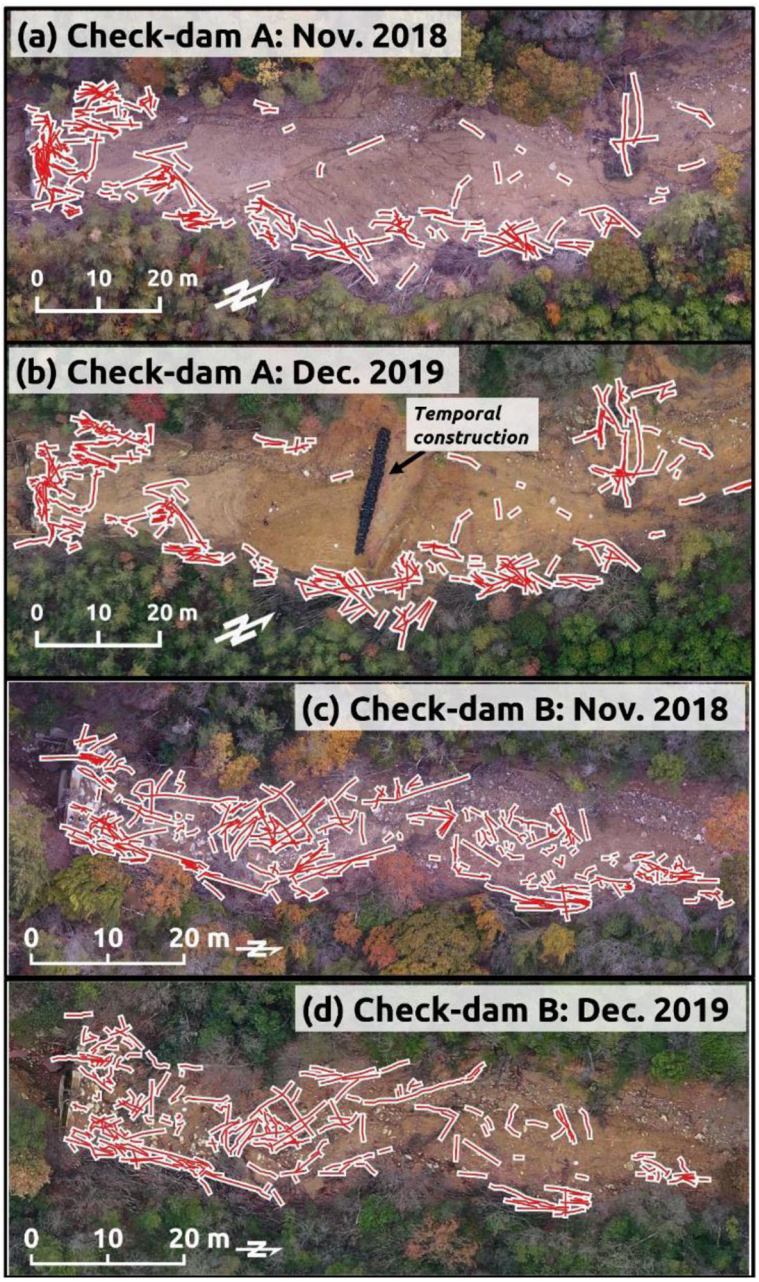

Fig. 11 Spatial distribution of extracted wood pieces at the broadleaf forest (BF) site: **a** check dam A on November 16, 2018, **b** check dam A on December 25, 2019, **c** check dam B on November 16, 2018, and **d** check-dam B on December 25, 2019

their lengths accurately using orthophotos acquired via UAVs. The lengths of most of the wood pieces originating from coniferous trees were measured with better than ±0.5 m accuracy using the orthophotos acquired by the UAV, but for the broadleaf trees, the lengths were underestimated systematically despite the absence of tree-crown coverage reducing the visibility (Figs. 4b and 5). Considering the complex structures of both ends of the broadleaf trees (i.e., wide and rounded crowns and root-wads; Fig. 3b), these underestimates may be attributed to missing extractions due to the low visibility of the broadleaf trees arising from the complex structures at the ends. In addition, the lengths of the entrapped wood pieces at the BF site was less than that at the CF site (Fig. 8), implying the fragmentation of broadleaf trees during the debris flow. Although the characteristics of the debris flow also probably influence the magnitude of wood-piece fragmentation (e.g., Johnson et al. 2000; Lancaster et al. 2003), the fragility of broadleaf trees may reduce the measurement accuracy based

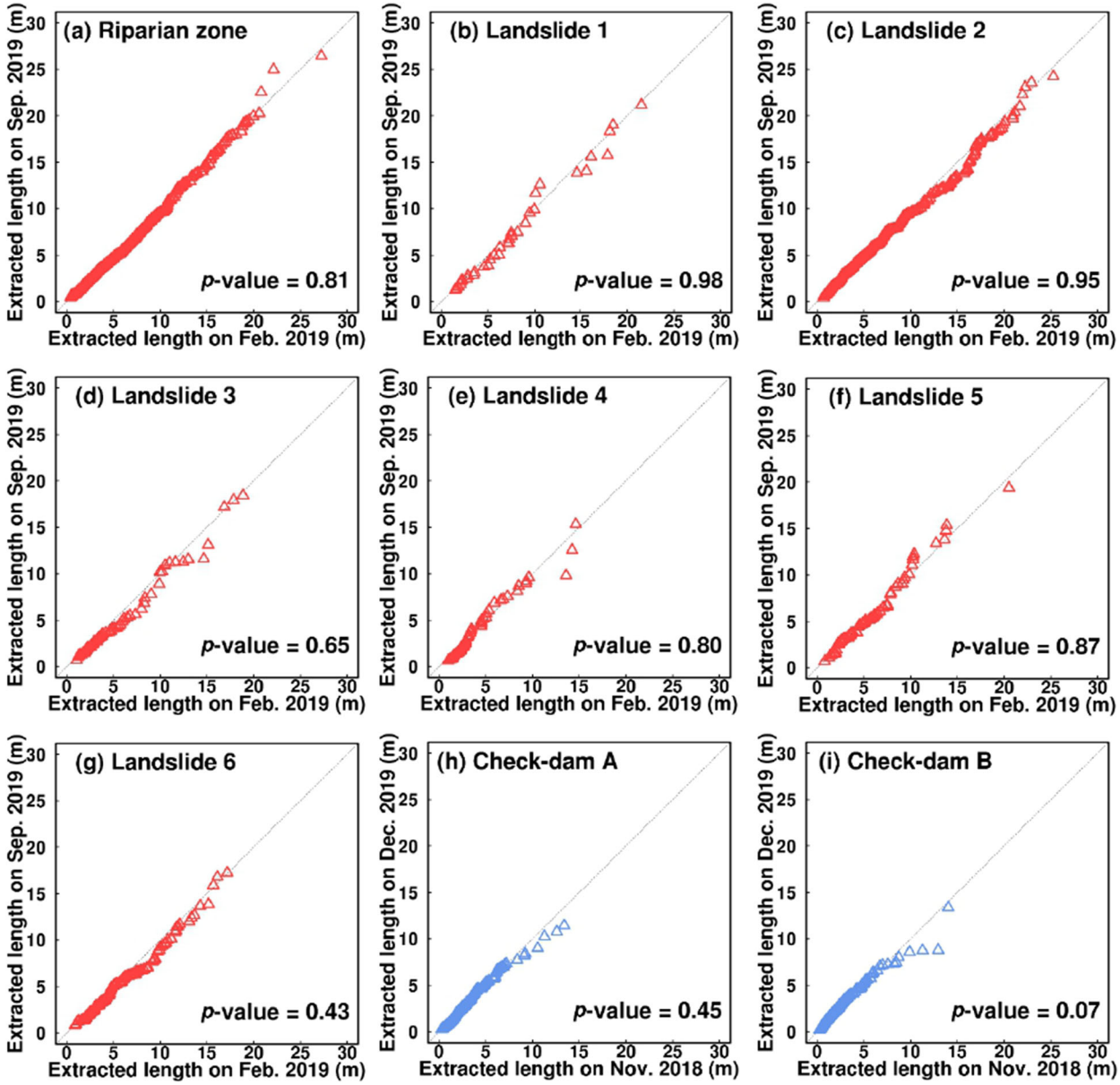

Fig. 12 Q–Q plots for the lengths of the extracted wood pieces: **a**–**g** the coniferous forest (CF) site and **h**–**i** the broadleaf forest (BF) site. The *p*-value indicates the result of the goodness-of-fit test (the Kolmogorov–Smirnov test)

on the orthophoto at the BF site by decreasing the visibility of the wood pieces.

Hence, most of the factors that decrease the measurement accuracy of wood pieces depend on visibility. Based on this interpretation, wood-piece measurements via UAV have both positive and negative aspects. Several components that affect the quality of the aerial photographs (e.g., black shadows, brightness involving overexposure, and insufficient overlap ratios among the aerial photographs) depend on the weather conditions and the flight plan (e.g., the path, height, and direction of shooting). For example, it is expected that low flight altitudes and flights under cloudy conditions can avoid block-out shadows and blown-out highlights in the acquired UAV images, resulting in an increase in the visibility of wood pieces in the processed orthophotos. Thus, an adequate flight plan may significantly improve the accuracy of UAV-based wood-piece measurements, without additional processing in the SfM-MVS photogrammetry.

Conversely, our results reveal an obvious limitation of orthophoto-based measurements. In general, wood

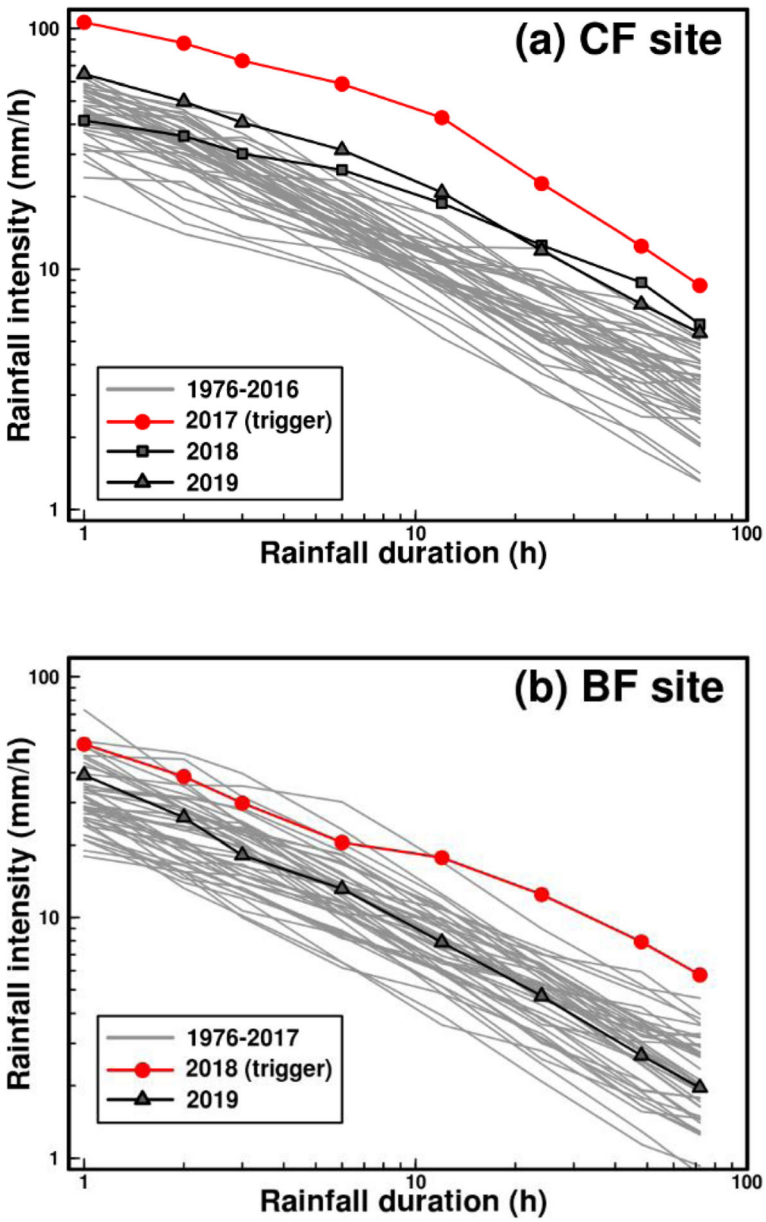

Fig. 13 Curves for the annual maxima of rainfall intensity: **a** the coniferous forest (CF) site and **b** the broadleaf forest (BF) site

Table 3 Return period (RP) for the annual maxima of rainfall intensities at the CF site

	RP_{1h} (year)	RP_{2h}	RP_{3h}	RP_{6h}	RP_{12h}	RP_{24h}	RP_{48h}	RP_{72h}
2017	> 100	> 100	> 100	> 100	> 100	> 100	> 100	> 100
2018	1.66	2.68	3.47	10.84	17.60	20.70	33.67	17.05
2019	10.32	11.98	14.18	33.46	32.22	15.86	11.17	11.31

pieces are not only dispersed along a channel but also result in logjam due to stacking and accumulation (e.g., Manners et al. 2007; Abalharth et al. 2015). However, the correlation between measurement accuracy and visibility from the sky demonstrates that the length

Table 4 Return period (RP) for the annual maxima of rainfall intensities at the BF site

	RP_{1h} (year)	RP_{2h}	RP_{3h}	RP_{6h}	RP_{12h}	RP_{24h}	RP_{48h}	RP_{72h}
2018	15.60	14.67	11.88	13.70	> 100	> 100	> 100	> 100
2019	3.77	2.76	1.90	2.36	2.13	2.00	1.77	1.67

measurements of wood pieces covered by a logjam are beyond the scope of orthophoto-based measurements. Sanhueza et al. (2019) pointed out that vegetation in streams also may cover wood pieces and thus decrease the measurement accuracy of wood pieces based on images acquired by UAV. Indeed, the tree-crown coverage decreased the measurement accuracy of wood-piece length (Fig. 4a). Given these measurement limitations, it is especially difficult to measure jam-forming wood pieces in streams deeply covered by vegetation (e.g., riparian trees) from the images acquired by a UAV.

In other words, the total number of wood pieces is probably underestimated in all UAV-based measurements. In this respect, the entrapment of wood pieces in landslide scars at the CF site may also have been underestimated, suggesting that high-ratio wood pieces were left even in slipped hillslopes. In some sub-watersheds with coniferous forests located around the CF site, no wood pieces were left in the landslide scars (Marutani et al. 2017). Thus, the difference in tree type (i.e., coniferous or broadleaf trees) cannot account for the high ratio of wood-piece entrapments in the landslide scars at the CF site compared with that at the BF site. The median length of wood pieces varied among landslide scars (Fig. 8a), probably depending on differences in runout processes and sediment volume among landslides. Considering this, the increase in the number of entrapped wood pieces with the increase in the landslide area (Fig. 9) indicates that wood pieces may remain in landslide scars regardless of differences in size and the dynamics of landslides. It seems that the outlets of landslide scars at the CF site are relatively narrow (like bottle-necked shapes) compared with those at the BF site (Fig. 2), which may lead to high-ratio wood-piece entrapments.

5.2 Possibility of the transport of the entrapped wood pieces

The slight changes in the lengths and spatial distributions of the wood pieces suggest that the wood pieces entrapped by the check dams were only slightly shifted by the debris-flow disaster (Figs. 10, 11, and 12). The elapsed time from the first flight was about 7 months for the CF site and over a year for the BF site (Table 2), which may be insufficient to cause significant visible decay. This means that intact wood pieces still remain in the upper reaches of the channels. However, considering the slight differences in the spatial distribution and Q–Q plot of the wood pieces at the CF site (Figs. 10 and 12), the high rainfall intensities in 2019 (Fig. 13a and Table 3) suggest that most of the entrapped wood pieces remain in place and rarely migrates, even when intense rainfall exceeding the level of the 30-year return period occurs. This implies that most rainfall events that do not cause debris flows and landslides cannot trigger secondary transport of entrapped wood pieces.

Because the pre-existing check dams trapped wood pieces at both sites, differences in the trend between such artificial trapping and natural entrapment of wood pieces should be noted. Even so, the low transportability of the entrapped wood pieces provides insight into the role of the wood pieces and sediment deposited in the upstream channel after debris flows and landslides. The efficacy of wood-piece trapping by closed-type check dams (check dams without slit and steel lattice structures) is generally considered relatively lower than that of open-type check dams (e.g., Piton and Recking 2016). Nevertheless, the entrapment of wood pieces by closed-type check dams continued in the long term, due to the low possibility of secondary transport at our study sites. May and Gresswell (2003b) argued that wood pieces in streams can facilitate sediment deposition, thereby resulting in an increase in sediment storage. Indeed, the low transportability of the entrapped wood pieces in the CF and BF sites indirectly indicates low erosion and discharge rates of the sediment stored after a landslide occurrence, suggesting that the entrapped wood pieces can impede subsequent sediment transport. For this reason, the trapping of wood pieces in low-order streams during and immediately after a landslide occurrence is important for mitigating subsequent impacts of the wood pieces and sediment on the facilities in residential regions.

6 Conclusions

We mapped wood pieces using orthophotos acquired by a UAV in two headwater channels covered by different forest types in Japan (coniferous and broadleaf forests at the CF and BF sites, respectively) after the landslide events due to heavy rainfall events in 2017 and 2018, respectively. The aims were twofold: (1) to determine whether or not ortho-photography acquired using a UAV allows measurements of wood-piece lengths based on comparisons between the UAV method and direct measurements and (2) to investigate whether entrapped wood pieces can be transported by intense rainfall.

At the CF site, comparing the directly measured lengths with the lengths extracted by UAV mapping indicates that aerial-photography measurements had approximately ±0.5 m accuracy when both ends of the wood pieces were satisfactorily visible. In contrast, some wood pieces were trapped by stand woods in the riparian zone, which were invisible underneath the tree crowns, and this led to underestimation of the extracted lengths. At the BF site, most of the extracted length values were shorter than the lengths measured directly, probably due to low visibility of the ends of the wood pieces due to complex tree structures in the root wads and tree

crowns. Hence, these results suggest that the measurement accuracy of wood pieces via UAV strongly depends on the visibility of the wood pieces arising from tree types. In other words, although flight operations that adequately increase the visibility of wood pieces in UAV images may improve the accuracy of wood-piece length measurements, the UAV-image-based approach is fundamentally inadequate for measuring jam-forming wood pieces, especially in streams covered by riparian trees.

Most wood pieces did not remain in the landslide scars at the BF site, whereas approximately 750 wood pieces were left in the landslide scars at the CF site. At the CF site, the number of remained wood pieces in the landslide scar tended to increase, depending on the increase in landslide area. Therefore, even large landslides cannot transport all wood pieces from their slip hillslopes in some cases, suggesting that wood pieces may remain in landslide scars regardless of the landslide area.

At both sites, changes in the frequency distribution of the lengths and the locations with respect to entrapped wood pieces were slight even over 7 months had passed since the first mapping. Nevertheless, at the CF site, some rainfall intensities between the two flights reached the second-highest values since 1976. Although the rainfall intensity that triggered the landslides in 2017 was higher than the annual maxima in 2019, some intensity values in 2019 exceeded the 30-year return period. This suggests that most of the entrapped wood pieces in any entrapment area remain and rarely re-migrate, even under intense rainfall.

Abbreviations

BF: Broadleaf forest; CF: Coniferous forest; GCP: Ground-control point; GNSS: Global navigation satellite system; LiDAR: Light detection and ranging; RTK: Real time kinematic; SfM-MVS: Structure from motion multiview stereo; UAV: Unmanned aerial vehicle

Acknowledgements

The authors are grateful to the staff of Forest Agency, Japan, for their assistance in the field observations. The constructive anonymous reviews and helpful comments from the editor significantly improved the quality of the paper and are greatly acknowledged.

Authors' contributions

HT conducted field measurements using a UAV and data analysis and drafted this manuscript. SM conducted field measurements and rainfall processing. SA, TO, and UK carried out field measurements. All authors read and approved the final manuscript.

Funding

This work was supported by the project "Development of technology for impacts, mitigation and adaptation to climate change in the sectors of agriculture, forestry and fisheries" of the Agriculture, Forestry, and Fisheries Research Council.

Availability of data and materials

The data used in this paper are available from the authors upon request.

Declarations

Competing interests

The authors declare that they have no competing interest.

Author details

[1]Forestry and Forest Products Research Institute, 1, Matsunosato, Tsukuba, Ibaraki 305-8687, Japan. [2]Kyushu Research Center, Forestry and Forest Products Research Institute, 4-11-16, Kurokami, Kumamoto, Kumamoto 860-0862, Japan.

Received: 27 August 2020 Accepted: 12 March 2021
Published online: 26 March 2021

References

Abalharth M, Hassan M, Klinkenberg B, Leung V, McCleary R (2015) Using LiDAR to characterize logjams in lowland rivers. Geomorphology 246:531–541. https://doi.org/10.1016/j.geomorph.2015.06.036

Atha JB (2013) Identification of fluvial wood using Google Earth. River Research and Applications 30:857–864

Atha JB, Dietrich JT (2016) Detecting fluvial wood in forested watersheds using LiDAR data: a methodological assessment. River Research and Applications 32(7):1587–1596. https://doi.org/10.1002/rra.2989

Barnhart KR, Rengers FK, Ghent JN, Tucker GE, Coe JA, Kean JW, Smith JB, Staley DM, Kleiber W, Wiens AM (2019) Topographic change detection at Chalk Cliffs, Colorado, USA, using Airborne LiDAR and UAS-based Structure-from-Motion photogrammetry. In: Kean JW, Coe JA, Santi PM, and Guillen BK (eds) Debris-flow hazards mitigation: mechanics, monitoring, modeling, and assessment, Association of Environmental and Engineering Geologists, Special Publication #28, pp 85–92.

Booth AM, Sifford C, Vascik B, Siebert C, Buma B (2020) Large wood inhibits debris flow runout in forested southeast Alaska. Earth Surface Processes and Landforms 45(7):1555–1568. https://doi.org/10.1002/esp.4830

Carbonneau PE, Dietrich JT (2017) Cost-effective non-metric photogrammetry from consumer-grade sUAS: implications for direct georeferencing of structure from motion photogrammetry. Earth Surface Processes and Landforms 42(3):473–486. https://doi.org/10.1002/esp.4012

Chigira M, Ling S, Matsushi Y (2018) Landslide disaster induced by the 2017 northern Kyushu rainstorm. Disaster Prevention Research Institute Annals, A 61:28–35 (in Japanese, with English abstract).

Comiti F, Andreoli A, Lenzi MA, Mao L (2006) Spatial density and characteristics of woody debris in five mountain rivers of the dolomites (Italian Alps). Geomorphology 78(1-2):44–63. https://doi.org/10.1016/j.geomorph.2006.01.021

Fonstad MA, Dietrich JT, Courville BC, Jensen JL, Carbonneau PE (2013) Topographic structure from motion: a new development in photogrammetric measurement. Earth Surface Processes and Landforms 38:755–766

Gurnell AM, Petts GE, Hannah DM, Smith BPG, Edwards PJ, Kollmann J, Ward JV, Tockner K (2001) Riparian vegetation and island formation along the gravel-bed Riume Tagliamento, Italy. Earth Surface Processes and Landforms 26(1):31–62. https://doi.org/10.1002/1096-9837(200101)26:1<31::AID-ESP155>3.0.CO;2-Y

Haga H, Kumagai T, Otsuki K, Ogawa S (2002) Transport and retention of coarse woody debris in mountain streams: an in situ field experiment of log transport and a field survey of coarse woody debris distribution. Water Resource Research 38(8):1-1–1-16.

Imada Y, Kawase H, Watanabe M, Arai M, Shiogama H, Takayabu I (2020) Advanced risk-based event attribution for heavy regional rainfall events. npj Climate and Atmospheric Science 3:37.

Jackson CR, Sturm CA (2002) Woody debris and channel morphology in first and second order forested channels in Washington's coast ranges. Water Resource Research 38:1177–1190

James MR, Robson S (2014) Mitigating systematic error in topographic models derived from UAV and ground-based image networks. Earth Surface Processes and Landforms 39(10):1413–1420. https://doi.org/10.1002/esp.3609

Johnson AC, Swanston DN, McGee KE (2000) Landslide initiation, runout, and deposition within clearcuts and old-growth forests of Alaska. Journal of the American Water Resources Association 36(1):17–30. https://doi.org/10.1111/j.1752-1688.2000.tb04245.x

Kaibori M, Hasegawa Y, Yamashita Y, Sakida H, Nakai S, Kuwada S, Hiramatsu S, Jitousono T, Irasawa M, Shimizu O, Imaizumi F, Nakatani K, Kashiwabara Y, Kato N, Torita E, Hirakawa Y, Yoshinaga S, Tanaka K, Hayashi S (2018) Sediment related disaster due to heavy rainfall in Hiroshima prefecture in July, 2018. Journal of the Japan Society of Erosion Control Engineering 71:43–53 (in Japanese, with English abstract).

Kasprak A, Magilligan FJ, Nislow KH, Snyder NP (2012) A Lidar-derived evaluation of watershed-scale large woody debris sources and recruitment mechanisms: coastal Maine, USA. River Research and Applications 28(9):1462–1476. https://doi.org/10.1002/rra.1532

Kato R, Shimose K, Shimizu S (2018) Predictability of precipitation caused by linear precipitation systems during the July 2017 Northern Kyushu heavy rainfall event using a cloud-resolving numerical weather prediction model. Journal of Disaster Research 13(5):846–859. https://doi.org/10.20965/jdr.2018.p0846

Keller EA, Swanson FJ (1979) Effects of large organic material on channel form and fluvial processes. Earth Surface Processes 4(4):361–380. https://doi.org/10.1002/esp.3290040406

Koutsoyiannis D, Kozonis D, Manetas A (1998) A mathematical framework for studying rainfall intensity-duration-frequency relationships. Journal of Hydrology 206(1-2):118–135. https://doi.org/10.1016/S0022-1694(98)00097-3

Lancaster ST, Hayes SK, Grant GE (2003) Effects of wood on debris flow runout in small mountain watersheds. Water Resources Research 39:1168

Lisle TE (1995) Effects of coarse woody debris and its removal on a channel affected by the 1980 eruption of Mount St. Helens, Washington. Water Resources Research 31(7):1797–1808. https://doi.org/10.1029/95WR00734

Manners RB, Doyle MW, Small MJ (2007) Structure and hydraulics of natural woody debris jams. Water Resources Research 43:W06432

Marutani T, Kaibori M, Jitousono T, Mizuno H, Ohno H, Shimizu O, Kubota T, Ue H, Kanazawa A, Kawano T, Koga S, Kobayashi H, Kobayashi T, Sakashima T, Sakatani Y, Sagara W, Shinohara Y, Suzuki Y, Takagi M, Torita E, Nakano K, Fujisawa Y, Yamaguchi K, Yamada Y (2017) Sediment-related disasters by a heavy rainfall in the northern part of Kyushu-Island, Japan in July 2017. Journal of the Japan Society of Erosion Control Engineering 70: 31–42 (in Japanese, with English abstract).

May CL (2002) Debris flows through different forest age classes in the central Oregon Coast Range. Journal of the American Water Resources Association 38(4):1097–1113. https://doi.org/10.1111/j.1752-1688.2002.tb05549.x

May CL, Gresswell RE (2003a) Large wood recruitment and redistribution in headwater streams in the Southern Oregon Coast Range, USA. Canadian Journal of Forest Research 33(8):1352–1362. https://doi.org/10.1139/x03-023

May CL, Gresswell RE (2003b) Processes and rates of sediment and wood accumulation in headwater streams of the Oregon Coast Range, USA. Earth Surface Processes and Landforms 28(4):409–424. https://doi.org/10.1002/esp.450

Montgomery DR, Abbe TB, Peterson NP, Buffington JM, Schmidt K, Stock JD (1996) Distribution of bedrock and alluvial channels in forested mountain drainage basins. Nature 381(6583):587–589. https://doi.org/10.1038/381587a0

Montgomery DR, Buffington JM, Smith R, Schmidt K, Pess G (1995) Pool spacing in forest channels. Water Resources Research 31(4):1097–1105. https://doi.org/10.1029/94WR03285

Nakamura F, J-Il S, Akasaka T, Swanson FJ (2017) Large wood, sediment, and flow regimes: their interactions and temporal changes caused by human impacts in Japan. Geomorphology 279:176–187. https://doi.org/10.1016/j.geomorph.2016.09.001

Nakamura F, Swanson FJ (1993) Effects of coarse woody debris on morphology and sediment storage of a mountain stream system in western Oregon. Earth Surface Processes and Landforms 18(1):43–61. https://doi.org/10.1002/esp.3290180104

Piton G, Recking A (2016) Design of sediment traps with open check dams. II: woody debris. Journal of Hydraulic Engineering 142:1–17

Ravazzolo D, Mao L, Picco L, Lenzi MA (2015) Tracking log displacement during floods in the Tagliamento River using RFID and GPS tracker devices. Geomorphology 228:226–233. https://doi.org/10.1016/j.geomorph.2014.09.012

Ruiz-Villanueva V, Bodoque JM, Díez-Herrero A, Eguibar MA, Pardo-Igúzquiza E (2013) Reconstruction of a flash flood with large wood transport and its influence on hazard patterns in an ungauged mountain basin. Hydrological Processes 27(24):3424–3437. https://doi.org/10.1002/hyp.9433

Ruiz-Villanueva V, Piégay H, Gurnell AM, Marston RA, Stoffel M (2016) Recent advances quantifying the large wood dynamics in river basins: new methods and remaining challenges. Reviews of Geophysics 54(3):611–652. https://doi.org/10.1002/2015RG000514

Sane Y, Panthou G, Bodian A, Vischel T, Lebel T, Dacosta H, Quantin G, Wilcox C, Ndiaye O, Diongue-Niang A, Kane MD (2018) Intensity–duration–frequency (IDF) rainfall curves in Senegal. Natural Hazards and Earth System Sciences 18(7):1849–1866. https://doi.org/10.5194/nhess-18-1849-2018

Sanhueza D, Picco L, Ruiz-Villanueva V, Iroumé A, Ulloa H, Barrientos G (2019) Quantification of fluvial wood using UAVs and structure from motion. Geomorphology 345:106837. https://doi.org/10.1016/j.geomorph.2019.106837

Sueki K, Kajikawa Y (2019) Different precipitation systems between Hiroshima and Keihanshin during extreme rainfall event in western Japan in July 2018. Journal of the Meteorological Society of Japan 97(6):1221–1232. https://doi.org/10.2151/jmsj.2019-063

Swanson FJ, Gregory SV, Iroumé A, Ruiz-Villanueva V, Wohl E (2021) Reflection on the history of research on large wood in rivers. Earth Surface Processes and Landforms 46(1):55–56. https://doi.org/10.1002/esp.4814

Tang YJ, Xu ZM, Yang TQ, Zhou ZH, Wang K, Ren Z, Yang K, Tian L (2018) Impacts of small woody debris on slurrying, persistence, and propagation in a low-gradient channel of the Dongyuege debris flow in Nu River, Southwest China. Landslides 15(11):2279–2293. https://doi.org/10.1007/s10346-018-1036-7

Tsuguti H, Seino N, Kawase H, Imada Y, Nakaegawa T, Takayabu I (2019) Meteorological overview and mesoscale characteristics of the Heavy Rain Event of July 2018 in Japan. Landslides 16(2):363–371. https://doi.org/10.1007/s10346-018-1098-6

Tsuji H, Yokoyama C, Takayabu YN (2020) Contrasting features of the July 2018 heavy rainfall event and the 2017 Northern Kyushu rainfall event in Japan. Journal of the Meteorological Society of Japan 98(4):859–876. https://doi.org/10.2151/jmsj.2020-045

Tsunetaka H, Hotta N, Hayakawa YS, Imaizumi F (2020) Spatial accuracy assessment of unmanned aerial vehicle-based structures from motion multi-view stereo photogrammetry for geomorphic observations in initiation zones of debris flows, Ohya landslide, Japan. Progress in Earth and Planetary Science 7: doi https://doi.org/10.1186/s40645-020-00336-0

Ulloa H, Iroumé A, Mao L, Andreoli A, Diez S, Lara LE (2015) Use of remote imagery to analyse changes in morphology and longitudinal large wood distribution in the Blanco River after the 2008 Chaitén volcanic eruption, southern Chile. Geografiska Annaler: Series A, Physical Geography 97(3):523–541. https://doi.org/10.1111/geoa.12091

Unuma T, Takemi T (2021) Rainfall characteristics and their environmental conditions during the heavy rainfall events over Japan in July of 2017 and 2018. Journal of the Meteorological Society of Japan (in press).

Wallace JB, Benke AC (1984) Quantification of wood habitat in subtropical coastal plain streams. Canadian Journal of Fisheries and Aquatic Science 41:1643–1652.

Woodsmith RD, Buffington JM (1996) Multivariate geomorphic analysis of forest streams: implications for assessment of land use impact on channel condition. Earth Surface Processes and Landforms 21(4):377–393. https://doi.org/10.1002/(SICI)1096-9837(199604)21:4<377::AID-ESP546>3.0.CO;2-2

Wyżga B, Mikuś P, Zawiejska J, Ruiz-villanueva V, Kaczka RJ, Czech W (2017) Log transport and deposition in incised, channelized, and multithread reaches of a wide mountain river: tracking experiment during a 20-year flood. Geomorphology 279:98–111. https://doi.org/10.1016/j.geomorph.2016.09.019

Publisher's Note